Numerical Analysis of Large Axisymmetric Deformations of Thin Spherical Shells

PAUL E. WILSON* AND EDWARD E. SPIER*
General Dynamics/Astronautics, San Diego, Calif.

Nonlinear difference equations for the numerical analysis of large axisymmetric deflections of thin linearly elastic and isotropic spherical shells are presented. Surface loading, temperature, and shell thickness may vary along a generator, and, in addition, temperature may vary through the thickness. The difference equations, which govern a stress function and the rotation of a meridional tangent, are written in a convenient matrix form and solved by combining an iterative scheme with a direct elimination method. The general theory is programed on an IBM 7090 digital computer, and important aspects of the input-output formats are explained. A nonclassical problem involving a "deep" spherical shell of variable thickness subjected to "thermal" pressure and edge loading is solved by means of the computer program. For this problem it was found that linear theory generally gave very conservative results. In addition, the problem of a spherical shell subjected to a concentrated load at the apex is treated, and certain of the numerical results are verified experimentally.

Nomenclature

a	= radius of spherical shell
a, b	= matrices that characterize boundary conditions at $n = 1$
a_1, a_2, b_1, b_2	= elements of matrices a, b
A, B	= relations that characterize temperature distribution
A_n, B_n, C_n	= matrices that define variable coefficients of difference equations
d, e	= matrices that characterize boundary conditions at $n = N$
d_1, d_2, e_1, e_2	= elements of matrices d, e
E	= modulus of elasticity
f_n	= matrices that define right-hand side of difference equations
f_1, f_2	= elements of f_n matrix
F_n	= quantity given by Eq. (39)
g_n	= quantity given by second of Eqs. (9)
h	= shell thickness
$\bar{h}$	= h/h_1
H, V	= radial and axial stress resultants
I	= identity matrix
k	= coefficient of thermal expansion
m	= number of iterations to convergence
M_T, N_T	= quantities given by Eqs. (2)
M_ξ, M_θ	= meridional and hoop stress couples
n	= arbitrary mesh point
N	= terminal mesh point, also stress resultant at apex
N_ξ, N_θ, Q	= meridional, hoop, and shearing stress resultants
$0(\beta^2)$	= quantity of order β^2
p	= pressure loading
p_H, p_V	= radial and axial components of middle surface load intensity
P	= concentrated load at apex of closed shell
P_n	= two by two coefficient matrix
$P_{11}, P_{12}, P_{21}, P_{22}$	= elements of P_n matrix
r_0, z_0	= radial and axial coordinates of undeformed middle surface
q_n	= column vector of loads and nonlinear terms
q_1, q_2	= elements of q_n column vector
r, θ, z	= cylindrical coordinates
s	= arc length measured along middle surface of shell generator
Δs	= distance between two adjoining mesh points on shell middle surface
$\overline{\Delta s}$	= $\Delta s/h_1$
T	= temperature above some fixed datum
u, w	= radial and axial displacement components
x, y, z	= rectangular Cartesian coordinates
y_n	= column vector giving ψ_n and β_n
$\alpha_i;\ i = 1, 2, \ldots, 5$	= variable coefficients of difference equations
β	= rotation of meridional tangent
δ_1, δ_2	= relations given by Eqs. (11)
μ^2	= $12(1 - \nu^2)$
ν	= Poisson's ratio
ξ, θ, ζ	= orthogonal curvilinear shell coordinates
ρ	= radius-thickness ratio, a/h
$\sigma_\xi, \sigma_\theta$	= meridional and hoop stresses
φ	= colatitude angle of normal to deformed shell
φ_0	= colatitude angle of normal to undeformed shell
Ψ	= dimensionless stress function
$(\ )'$	= derivative of quantity in parenthesis with respect to s
$(\ )^{-1}$	= inverse of quantity in parenthesis
$(\sim)$	= pure nonlinear term; for certain loads V, p_H, p_V may also be "nonlinear"
$\begin{Bmatrix} L_1 \\ L_2 \\ L_3 \end{Bmatrix}$	= take (L_1, L_2, L_3) at points $(n = 1, n, N)$, respectively

Presented as Preprint 64-440 at the 1st AIAA Annual Meeting, Washington, D. C., June 29–July 2, 1964; revision received May 13, 1965. This work was supported by General Dynamics/Astronautics under research program No. 111-9582. The authors extend their appreciation to M. M. Thorn and H. W. Rose for programing the equations presented in this paper and thank D. R. Cropper, E. M. Slick, and M. A. Kirk for assisting in various phases of the work. Thanks are also extended to J. W. Fortenberry and J. Bodenham for supplying the experimental results and to others at General Dynamics/Astronautics who had a part in this work.

* Design Specialist, Structures Research. Member AIAA.

I. Introduction

MANY areas of research are required to provide information necessary for the design of aerospace vehicles incorporating thin-walled shell structures. This paper investigates one of these areas, namely, the numerical analysis of large axisymmetric deflections of thin spherical shells. A problem of this type requires the integration of a rather complicated system of simultaneous nonlinear differential equations. Unfortunately, because of integration difficulties, analytical solutions presently in the literature are quite limited. Consequently, with the advent of large high-speed digital computers, the authors of several recent papers have focused their attention on methods of numerical integration of thin shell equations.

Several techniques for the numerical analysis of small deflections of various shells of revolution have been proposed.[1-8] In addition, various numerical methods for the analysis of large axisymmetric deflections of shells of revolution have been discussed recently.[9-18] However, specific nonlinear results have thus far been restricted primarily to shallow shells where intuitively small terms have been neglected in the governing differential equations.

Previously, the authors added thermal effects[13] to Reissner's[19,20] fourth-order system of two nonlinear differential equations that govern large axisymmetric deflections of thin linearly elastic and isotropic shells of revolution. These equations are coupled in a dimensionless stress function and the rotation of a meridional tangent and are sufficiently general so that surface loading, temperature, and shell thickness may vary along a meridian, and, in addition, temperature may vary through the thickness. First-order central difference approximations are used to reduce the two differential equations to finite-difference form. Then the resulting nonlinear difference equations are written in a convenient matrix form and solved by combining an iterative scheme with a direct elimination method that employs two by two coefficient matrices. The direct elimination method has been used earlier by Sepetoski[7] and Radkowski[8] in analyzing small axisymmetric deflections of shells of revolution. Also, working independently, Archer published[16] a similar numerical method for the analysis of large axisymmetric deflections of shells of revolution. He specializes the general theory to shallow spherical shells of constant thickness, omits certain intuitively negligible nonlinear terms from the differential equations, and considers the snap-through buckling of shallow spherical shells subjected to 1) uniform pressure and 2) a point load at the apex. His results are generally in favorable agreement with those given by earlier investigators.[21-25] However, Archer's analysis does not account for thermal stresses, and he does not give a numerical example for a "deep" spherical shell.

The purpose of this paper is to specialize the basic equations of Ref. 13 to a spherical shell and to present specific results that have been obtained by application of the numerical integration technique. These results help exemplify use of the method and confirm its ready applicability to a wide class of spherical shell problems that involve moderate nonlinearities. Since the basic nonlinear difference equations are written in nondimensional form, they suffice for parameter studies as well as for problems involving fixed geometries. These equations have been programed in Fortran language on an IBM 7090 digital computer.[15] In addition to core storage, the computer program uses 10 tapes and can accommodate as many as 20,000 mesh points. Necessary nondimensional input to the program consists of geometry, temperature parameters, physical loads, boundary conditions, and a suitable convergence tolerance. Output consists of linear and nonlinear values of the basic dependent variables along with appropriate components of displacement and stress.

A nonclassical problem involving a "deep" spherical shell of variable thickness with a hole at the apex is solved by means of the computer program. The edge near the apex is loaded by stress resultants and a stress couple, and the terminal edge of the shell is clamped. In addition, the shell is pressurized and subjected to a temperature distribution that varies both along the meridian and through the thickness. Nondimensional linear and nonlinear output data consisting of displacements and stresses are plotted vs the apex angle. It is shown that nonlinear effects are very important in a narrow edge-zone near the hole. For the loads considered, it was found that linear theory generally gives very conservative results. For example the maximum stress computed on the basis of linear theory is nearly 50% conservative.

Also, the large deflection of a nonshallow spherical shell (apex angle of 45°) of constant thickness subjected to a concentrated force at the apex is analyzed by means of the computer program. Radius-thickness ratios of 100, 600, 1080, and 3000 are considered. The numerical results for this problem point out the interesting fact that it is necessary to distinguish carefully between inward and outward bending (i.e., for outward loads linear theory is conservative, whereas for inward loads linear theory is often quite unconservative). Experimental load-deflection results obtained by the authors for spherical shells with radius-thickness ratios of 1080 and 6440 are shown to be in excellent agreement with the nonlinear numerical solution. When properly interpreted, certain of the results given here also may be shown to be in favorable agreement with those given earlier by Reissner[26] and Archer[16] in their respective treatments of the small and large deflections of shallow spherical shells (even though the shells considered here are not shallow).

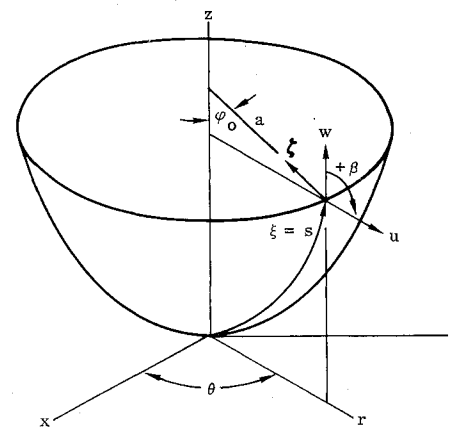

Fig. 1 Associated geometry and displacement components.

II. Summary of Theory

Geometry

Figure 1 shows the middle surface of a thin spherical shell of radius a and variable thickness h. Let (x, y, z), (r, θ, z), and (ξ, θ, ζ) denote rectangular Cartesian, cylindrical, and orthogonal shell coordinates, respectively. It is convenient to select $\xi = s$ where s is the arc length measured along a generator and to let φ_0 represent the angle between a normal to the undeformed reference surface and the z axis. Postulate that (u, w) represent displacement components in the positive (r, z) directions, respectively, and let β denote the rotation of a meridional tangent taken positive as shown in Fig. 1. Consequently it follows that

$$\varphi_0 = s/a \qquad r_0 = a \sin\varphi_0$$
$$z_0 = a(1 - \cos\varphi_0) \tag{1}$$

where (r_0, z_0) are the radial (horizontal) and axial (vertical) coordinates of the undeformed middle surface, respectively.

Stress Resultants

Stress resultants (N_ξ, N_θ, Q) and stress couples (M_ξ, M_θ) are defined in the usual way[20] and are taken positive when acting as shown in Fig. 2. In addition, it is convenient to define stress resultants (H, V) and components of middle surface load intensity (p_H, p_V) that act in the positive (r, z) coordinate directions, respectively (Fig. 2). Quantities N_T and M_T that arise because of thermal effects are defined as follows:

$$N_T = \int_{-h/2}^{h/2} EkT\, d\zeta \qquad M_T = \int_{-h/2}^{h/2} EkT\, \zeta d\zeta \tag{2}$$

where E is the modulus of elasticity, k is the coefficient of

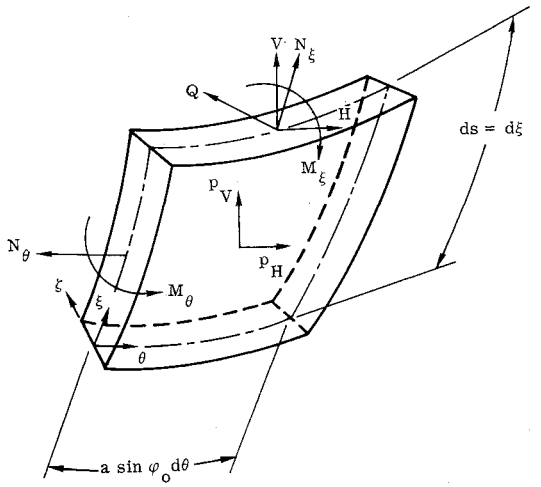

Fig. 2 Element of shell showing stress resultants, stress couples, and surface loads.

thermal expansion, and T is the temperature above some fixed datum. Also, rather than treating H as a dependent variable, it is convenient to introduce a dimensionless stress function Ψ as follows[8]:

$$\Psi = \mu\rho(H/Eh)\sin\varphi_0 \tag{3}$$

$$\mu^2 = 12(1-\nu^2) \qquad \rho = a/h \tag{4}$$

where ν is Poisson's ratio.

Difference Equations

Let $n(n = 1, 2, 3, \ldots, N)$ denote a generic point on the generator of the spherical shell shown in Fig. 3, and let the shell be divided into $(N-1)$ segments of equal length Δs. By using first-order central differences, the differential equations of equilibrium and compatibility that govern small finite axisymmetric deformations of thin spherical shells may be written as follows[13,15]:

$$\left.\begin{aligned}\alpha_1\Psi_{n+1} + \alpha_2\Psi_n + \alpha_3\Psi_{n-1} + \alpha_4\beta_n &= f_1\\ \alpha_1\beta_{n+1} + \alpha_5\beta_n + \alpha_3\beta_{n-1} - \alpha_4\Psi_n &= f_2\end{aligned}\right\} n = 2, 3, \ldots, N-1 \tag{5}$$

where

$$\left.\begin{aligned}\alpha_1 &= 1 + (\overline{\Delta s}/2\bar{h})\,[(1/\rho)\cot\varphi_0 + 3h']\\ \alpha_2 &= -2 + (\overline{\Delta s}/\bar{h})^2[(1/\rho^2)(\nu - \cot^2\varphi_0) + 2hh'' + (2+\nu)(h'/\rho)\cot\varphi_0]\\ \alpha_3 &= 1 - \frac{\overline{\Delta s}}{2\bar{h}}\left(\frac{1}{\rho}\cot\varphi_0 + 3h'\right) \qquad \alpha_4 = -\frac{\mu}{\rho}\left(\frac{\overline{\Delta s}}{\bar{h}}\right)^2\\ \alpha_5 &= -2 - (\overline{\Delta s}/\rho\bar{h})^2\,(\nu + \cot^2\varphi_0 - 3\nu\rho h'\cot\varphi_0)\end{aligned}\right\} \tag{6}$$

$$\begin{aligned}f_1 = \mu\left(\frac{\overline{\Delta}}{\bar{h}}\right)^2\Bigg[&\frac{1}{\rho}\,[(1+2\nu)\cos\varphi_0 - \nu\rho h'\sin\varphi_0]\,\frac{V}{Eh} + \nu\frac{V'}{E}\sin\varphi_0 - [(2+\nu)\cos\varphi_0 - \rho h'\sin\varphi_0]\,\frac{p_H}{E} - \rho\frac{hp_H'}{E}\sin\varphi_0 + h'\frac{N_T}{Eh} - \frac{N_T'}{E} +\\ &\tilde{\beta}\Bigg\{\frac{1}{\mu\rho^2}\,[(2+\nu)\cot\varphi_0 - \nu\rho h']\,\Psi - \nu\frac{V'}{E}\cos\varphi_0 - \nu\frac{p_H}{E}\sin\varphi_0 + \frac{1}{\rho}\frac{N_T}{Eh} + \frac{1}{\rho}\,[(1+\nu)(1-\cot^2\varphi_0)\sin\varphi_0 + \nu\rho h'\cos\varphi_0]\,\frac{V}{Eh}\Bigg\} - \frac{\tilde{\beta}^2}{2\rho}\cot\varphi_0 + \nu h\tilde{\beta}'\left(\frac{\Psi}{\mu\rho} - \frac{V}{Eh}\cos\varphi_0\right)\Bigg]\end{aligned} \tag{7}$$

$$\begin{aligned}f_2 = \left(\frac{\mu\overline{\Delta s}}{\bar{h}}\right)^2\Bigg\{&\frac{V}{Eh}\cos\varphi_0 + \frac{1}{1-\nu}\frac{M_T'}{Eh} + \tilde{\beta}\Bigg[\frac{\Psi}{\mu\rho}\cot\varphi_0 + \frac{V}{Eh}\sin\varphi_0 - \frac{1}{\rho(1-\nu)}\frac{M_T}{Eh^2}\Bigg] + \frac{\tilde{\beta}^2}{\mu^2}\Bigg[\frac{3-\nu}{2\rho^2}\cot\varphi_0 + \frac{6(1+\nu)}{\rho}\frac{M_T}{Eh^2}\cot\varphi_0 - \frac{3\nu h'}{2\rho}\Bigg]\Bigg\}\end{aligned} \tag{8}$$

where

$$\left.\begin{aligned}\frac{V}{Eh} &= -\frac{\delta_1}{2\pi\rho\sin\varphi_0}\cdot\frac{P}{Eh^2} + \frac{\delta_2}{\bar{h}}\frac{V_1}{Eh_1}\frac{(\sin\varphi_0)_1}{\sin\varphi_0} - \frac{\overline{\Delta s}}{\bar{h}}\frac{1}{\sin\varphi_0}\left[\frac{1}{2}(g_1 + g_n) + \sum_{i=2}^{i=n-1} g_i\right]\\ g_n &= (p_V/E)\sin\varphi_0\\ V'/E &= -(V/Eh)\,(\cot\varphi_0/\rho) - (p_V/E)\\ h\beta' &= (\bar{h}/2\overline{\Delta s})(\beta_{n+1} - \beta_{n-1})\end{aligned}\right\} \tag{9}$$

and

$$\left.\begin{aligned}\varphi_0 &= (\varphi_0)_1 + (\overline{\Delta s}/\rho_1)(n-1)\\ N &= 1 + (\rho_1/\overline{\Delta s})[(\varphi_0)_N - (\varphi_0)_1]\\ \bar{h} = h/h_1 \qquad \overline{\Delta s} &= (\Delta s/h_1) \qquad (\ )' = (d/ds)(\ )\end{aligned}\right\} \tag{10}$$

and, in addition,

$$\delta_1 = 0 \qquad \delta_2 = 1 \qquad \text{shell open at apex} \tag{11}$$

$$\delta_1 = 1 \qquad \delta_2 = 0 \qquad \text{shell closed at apex}$$

Here P denotes a concentrated load, which acts at the apex (if one exists) in the direction of positive z, and expressions involving the terms ($\sim$) indicate "pure" nonlinear quantities. If it is assumed that h, p_H, N_T, and M_T are known explicitly as a function of s, then expressions for the derivatives of these quantities may be evaluated directly. In the event that h, p_H, N_T, and M_T are known only at the grid points n, then expressions for their derivatives may be deduced by relations similar to the last of Eqs. (9). For compactness of notation it should be noted that in Eqs. (5–10) the subscript n usually has been omitted in the expressions for (α_i, f_i, h, $\bar{h}$, ρ, φ_0, V, p_H, p_V, N_T, M_T, β, Ψ). This policy will be continued in subsequent work where the meaning is clear.

Boundary Conditions

For most applications of the theory it suffices to specify on each edge (i.e., $n = 1$ or N) any two of the following: u or H and β or M_ξ. Consequently, by using first-order forward differences at the initial boundary, it is possible, within the framework of the present theory, to write the boundary conditions at $n = 1$ in the form

$$\Psi_1 + a_1\Psi_2 = b_1 \qquad \beta_1 + a_2\beta_2 = b_2 \tag{12}$$

where the following expressions for a_1, a_2, b_1, and b_2 are evaluated at $n = 1$:

$$u_1 \text{ specified}\left\{\begin{aligned}a_1 &= -1/1 + \overline{\Delta s}[(\nu\cot\varphi_0/\rho) - 2h']\\ b_1 &= a_1\mu\overline{\Delta s}\left[\frac{1}{\rho\sin\varphi_0}\frac{u}{\bar{h}} - \rho\frac{p_H}{E}\sin\varphi_0 + \nu\frac{V}{Eh}\sin\varphi_0 - \frac{N_T}{Eh} + \nu\tilde{\beta}\left(\frac{\Psi}{\mu\rho} - \frac{V}{Eh}\cos\varphi_0\right)\right]\end{aligned}\right\} \tag{13}$$

$$H_1 \text{ specified}\{a_1 = 0 \qquad b_1 = \mu\rho(H/Eh)\sin\varphi_0 \tag{14}$$

$$\beta_1 \text{ specified}\{a_2 = 0 \qquad b_2 = \beta \tag{15}$$

$$(M_\xi)_1 \text{ specified}\left\{\begin{aligned}a_2 &= -1/[1 - (\nu\overline{\Delta s}/\rho)\cot\varphi_0]\\ b_2 &= a_2\overline{\Delta s}\left[\mu^2\left(\frac{M_\xi}{Eh^2} + \frac{1}{1-\nu}\frac{M_T}{Eh^2}\right) - \frac{\nu\tilde{\beta}^2}{2\rho}\right]\end{aligned}\right\} \tag{16}$$

and for the apex of a closed shell,

$$a_1 = a_2 = b_1 = b_2 = 0 \tag{17}$$

Similarly, by using first-order backward differences at the terminal boundary, it is possible to write the boundary conditions at $n = N$ in the form

$$d_1\Psi_{N-1} + \Psi_N = e_1 \qquad d_2\beta_{N-1} + \beta_N = e_2 \tag{18}$$

where the following expressions for d_1, d_2, e_1, and e_2 are evaluated at $n = N$:

u_N specified

$$\begin{cases} d_1 = -1 \\ e_1 = -d_1\mu\dfrac{\overline{\Delta s}}{\bar{h}}\left[\dfrac{1}{\rho\sin\varphi_0}\dfrac{u}{\bar{h}} - \right. \\ \qquad \left. \rho\dfrac{p_H}{E}\sin\varphi_0 + \nu\dfrac{V}{Eh}\sin\varphi_0 - \dfrac{N_T}{Eh} + \right. \\ \qquad \left. \nu\tilde{\beta}\left(\dfrac{\Psi}{\mu\rho} - \dfrac{V}{Eh}\cos\varphi_0\right)\right] \end{cases} \tag{19}$$

$$\frac{1}{1 - (\overline{\Delta s}/\bar{h})[(\nu\cot\varphi_0/\rho) - 2h']}$$

H_N specified $\{d_1 = 0 \qquad e_1 = \mu\rho\,(H/Eh)\sin\varphi_0$ (20)

β_N specified $\{d_2 = 0 \qquad e_2 = \beta$ (21)

$(M_\xi)_N$ specified

$$\begin{cases} d_2 = -1/[1 + (\nu\overline{\Delta s}/\rho\bar{h})\cot\varphi_0] \\ e_2 = -d_2\dfrac{\overline{\Delta}}{\bar{h}}\left[\mu^2\left(\dfrac{M_\xi}{Eh^2} + \right.\right. \\ \qquad \left.\left.\dfrac{1}{1-\nu}\dfrac{M_T}{Eh^2}\right) - \dfrac{\nu\tilde{\beta}^2}{2\rho}\right] \end{cases} \tag{22}$$

Method of Solution

With Eqs. (5, 12, and 18), the fundamental numerical problem now may be posed, namely, to solve the $2N$ nonlinear difference equations

$$A_n y_{n+1} + B_n y_n + C_n y_{n-1} = f_n \qquad n = 2, 3, \ldots, N-1 \tag{23}$$

$$y_1 + ay_2 = b \qquad dy_{N-1} + y_N = e$$

for the $2N$ unknown values of Ψ_n and β_n, where

$$\left.\begin{aligned} A_n = \alpha_1 I,\ B_n = \begin{bmatrix} \alpha_2 & \alpha_4 \\ -\alpha_4 & \alpha_5 \end{bmatrix}\ C_n = \alpha_3 I \qquad I = \begin{bmatrix} 1 & 0 \\ 0 & 1 \end{bmatrix} \\ y_n = \begin{bmatrix} \Psi_n \\ \beta_n \end{bmatrix} \qquad f_n = \begin{bmatrix} f_1 \\ f_2 \end{bmatrix} \end{aligned}\right\} \tag{24}$$

$$\left.\begin{aligned} a = \begin{bmatrix} a_1 & 0 \\ 0 & a_2 \end{bmatrix} \qquad b = \begin{bmatrix} b_1 \\ b_2 \end{bmatrix} \\ d = \begin{bmatrix} d_1 & 0 \\ 0 & d_2 \end{bmatrix} \qquad e = \begin{bmatrix} e_1 \\ e_2 \end{bmatrix} \end{aligned}\right\} \tag{25}$$

A direct elimination method[27,28] that is well adapted for the solution of the linearized form of Eqs. (23) has been used (in essence) by several investigators[6-8,29] for the small deflection analysis of shells of revolution. In addition, this matrix method has been used in conjunction with various iteration schemes to investigate nonlinear phenomena concerning the large deflection,[13-15] buckling,[16] and plastic behavior[30] of various shells of revolution. The primary iteration scheme used in this paper for the solution of Eqs. (23) has been discussed previously in detail.[13] Accordingly, only pertinent aspects of the method are summarized as follows:

1) With a starting value of $P_1 = a$, compute the 2×2 coefficient matrices P_n ($n = 2, 3, \ldots, N-1$) from the formula

$$P_n = (B_n - C_nP_{n-1})^{-1}A_n \tag{26}$$

2) Then with a linearized starting value of $q_1 = b$, evaluate the 2×1 column vectors q_n ($n = 2, 3, \ldots, N-1$) from the relation

$$q_n = P_nA_n^{-1}(f_n - C_nq_{n-1}) \tag{27}$$

3) Calculate the linearized 2×1 column (solution) vectors y_n as indicated in the following:

$$y_N = (I - dP_{N-1})^{-1}(e - dq_{N-1})$$

$$y_{n-1} = q_{n-1} - P_{n-1}y_n \qquad n = N, N-1, \ldots, 2 \tag{28}$$

4) Use the linearized solution vector to obtain second approximations to f_n, b, e, q_n, and y_n, respectively.

5) Successively repeat step four and obtain third, fourth, ..., $(m-1)$th, and (m)th approximations to the desired nonlinear y_n solution vectors, and stop the iterative procedure when the difference between the (m)th and $(m-1)$th approximations to appropriate elements of the y_n solution vectors (or selected output quantities) is less than some suitable convergence criterion.

Numerical results presented in this paper indicate that the "simple" iteration scheme described previously is adequate for the evaluation of small nonlinearities. However, for the study of moderate nonlinearities, it has been found that it is necessary to use an "incremental" iteration method to achieve convergence. In this regard, certain of the results given in this paper for a spherical shell subjected to a concentrated load at the apex were obtained by the following iteration scheme: 1) use the "simple" iteration scheme described previously until a load parameter, say F, becomes large enough to cause slow convergence to the desired nonlinear solution; 2) to obtain the nonlinear solution for a larger load parameter $F + \Delta F$, increment the loads an amount ΔF and use the nonlinear values of y_n at load F and calculate the first nonlinear approximations to f_n, b, e, q_n, and y_n, respectively; 3) then compute second approximations to f_n, b, e, q_n, and y_n, respectively; 4) successively repeat step 3 until convergence is reached; and 5) repeat steps 2, 3, and 4 to obtain nonlinear solutions for larger loads.

For the evaluation of large nonlinearities, such as those that often occur during buckling and postbuckling phenomena, it is necessary to use a faster and more powerful iteration technique. In this regard Thurston's[11] accelerated Newtonian-type iteration scheme can be used.

Output Data

The y_n matrices will yield values of Ψ_n and β_n for $n = 1, 2, \ldots, N$, and the solution is complete except for the calculation of the customary output data. It may be shown[15] that the necessary formulas for the computation of stress resultants at

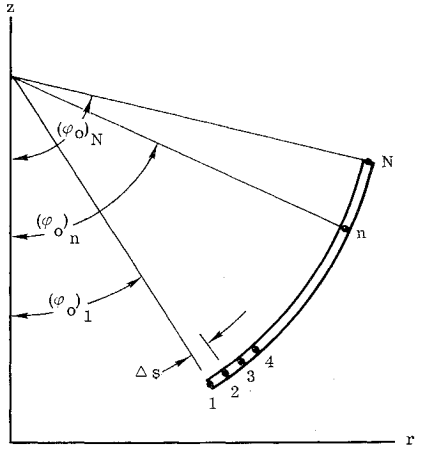

Fig. 3 Shell partitionment.

a generic point n are as follows:

$$\frac{N_\xi}{Eh} = \frac{\Psi}{\mu\rho}\cot\varphi_0 + \frac{V}{Eh}\sin\varphi_0 + \tilde{\beta}\left(\frac{\Psi}{\mu\rho} - \frac{V}{Eh}\cos\varphi_0\right) \quad (29)$$

$$\frac{N_\theta}{Eh} = \frac{1}{\mu\overline{\Delta s}}\begin{Bmatrix}(\Psi_2 - \Psi_1)\\ \frac{\bar{h}}{2}(\Psi_{n+1} - \Psi_{n-1})\\ \bar{h}(\Psi_N - \Psi_{N-1})\end{Bmatrix} + \frac{2h'\Psi}{\mu} + \rho\frac{p_H}{E}\sin\varphi_0 \quad (30)$$

$$\frac{M_\xi}{Eh^2} = \frac{1}{\mu^2\overline{\Delta s}}\begin{Bmatrix}(\beta_2 - \beta_1)\\ \frac{\bar{h}}{2}(\beta_{n+1} - \beta_{n-1})\\ \bar{h}(\beta_N - \beta_{N-1})\end{Bmatrix} + \frac{\nu\beta}{\mu^2\rho}\cot\varphi_0 - \frac{1}{1-\nu}\frac{M_T}{Eh^2} + \frac{\nu\tilde{\beta}^2}{2\mu^2\rho} \quad (31)$$

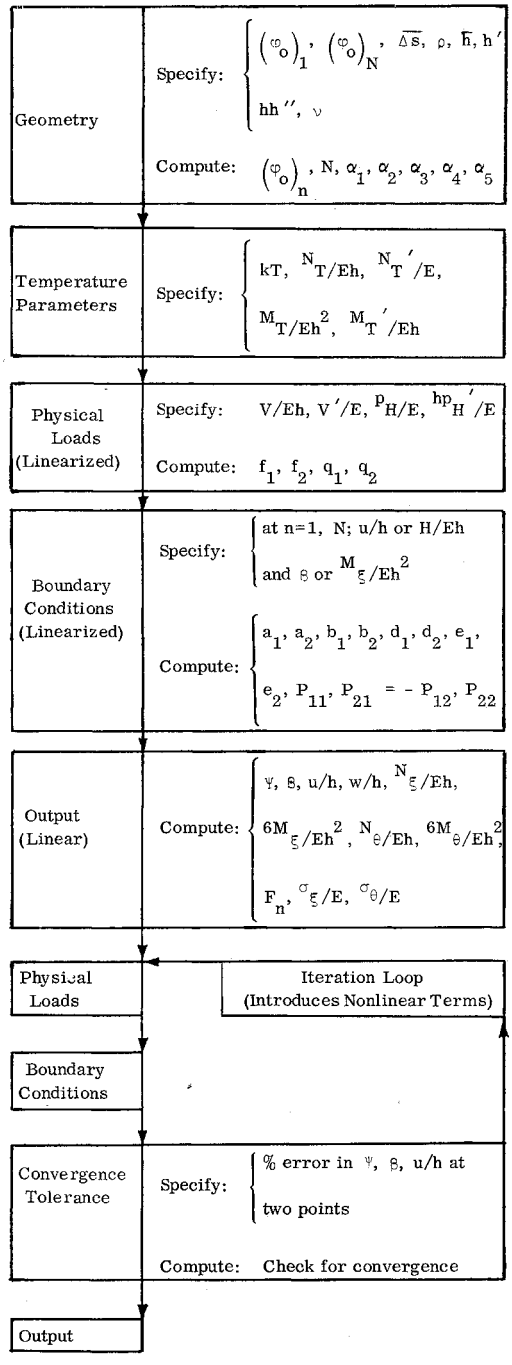

Fig. 4 Simplified flow diagram.

$$\frac{M_\theta}{Eh^2} = \frac{\nu}{\mu^2\overline{\Delta s}}\begin{Bmatrix}(\beta_2 - \beta_1)\\ \frac{\bar{h}}{2}(\beta_{n+1} - \beta_{n-1})\\ \bar{h}(\beta_N - \beta_{N-1})\end{Bmatrix} + \frac{\beta}{\mu^2\rho}\cot\varphi_0 - \frac{1}{1-\nu}\frac{M_T}{Eh^2} + \frac{\tilde{\beta}^2}{2\mu^2\rho} \quad (32)$$

For the apex $n = 1$ of a closed shell these become

$$\frac{N_\xi}{Eh} = \frac{N_\theta}{Eh} = \frac{\Psi_2}{\mu\overline{\Delta s}} - \frac{1}{2\pi}\left(\frac{1}{\rho} - \frac{\tilde{\beta}}{\overline{\Delta s}}\right)\frac{P}{Eh^2} \quad (33)$$

$$\frac{M_\xi}{Eh^2} = \frac{M_\theta}{Eh^2} = \frac{1}{1-\nu}\left(\frac{\beta_2}{12\overline{\Delta s}} - \frac{M_T}{Eh^2}\right) \quad (34)$$

Of course it should be noted that Eq. (34) is not valid if a concentrated load acts at the apex of a closed shell, since, for this circumstance, it is well known that M_ξ and M_θ are singular (i.e., unbounded) at $n = 1$.

With these values the stresses $(\sigma_\xi, \sigma_\theta)$ at point n may be computed from the relations

$$\frac{\sigma_\xi}{E} = \frac{N_\xi}{Eh} + \frac{1}{1-\nu}\frac{N_T}{Eh} + \frac{12\zeta}{h}\left(\frac{M_\xi}{Eh^2} + \frac{1}{1-\nu}\frac{M_T}{Eh^2}\right) - \frac{kT}{1-\nu} \quad (35)$$

$$\frac{\sigma_\theta}{E} = \frac{N_\theta}{Eh} + \frac{1}{1-\nu}\frac{N_T}{Eh} + \frac{12\zeta}{h}\left(\frac{M_\theta}{Eh^2} + \frac{1}{1-\nu}\frac{M_T}{Eh^2}\right) - \frac{kT}{1-\nu}$$

and the displacement components (u, w) at point n may be computed as follows:

$$\frac{u}{h} = \frac{\rho}{\mu}\sin\varphi_0\left[\frac{1}{\overline{\Delta s}}\begin{Bmatrix}(\Psi_2 - \Psi_1)\\ \frac{\bar{h}}{2}(\Psi_{n+1} - \Psi_{n-1})\\ \bar{h}(\Psi_N - \Psi_{N-1})\end{Bmatrix} + 2h'\Psi - \frac{\nu\Psi}{\rho}\cot\varphi_0 - \nu\mu\frac{V}{Eh}\sin\varphi_0 + \mu\rho\frac{p_H}{E}\sin\varphi_0 + \mu\frac{N_T}{Eh} - \nu\tilde{\beta}\left(\frac{\Psi}{\rho} - \mu\frac{V}{Eh}\cos\varphi_0\right)\right] \quad (36)$$

Usually it is sufficient to specify either $w_1 = 0$ or $w_N = 0$. If $w_1 = 0$, then

$$w_2/h_2 = \tfrac{1}{2}(\overline{\Delta s}/\bar{h}_2)(F_1 + F_2)$$

$$\frac{w}{h} = \frac{\overline{\Delta s}}{\bar{h}}\left[\frac{1}{2}(F_1 + F_n) + \sum_{i=2}^{i=n-1} F_i\right] \qquad n = 3, 4, \ldots, N \quad (37)$$

and if $w_N = 0$, then

$$\left.\begin{aligned}\frac{w_1}{h_1} &= -\overline{\Delta s}\left[\frac{1}{2}(F_1 + F_N) + \sum_{i=2}^{i=N-1} F_i\right]\\ \frac{w_2}{h_2} &= \frac{\overline{\Delta s}}{\bar{h}_2}\left[\frac{1}{2}(F_2 - F_N) - \sum_{i=2}^{i=N-1} F_i\right]\\ \frac{w}{h} &= \frac{\overline{\Delta s}}{\bar{h}}\left[\frac{1}{2}(F_n - F_N) + \sum_{i=2}^{i=n-1} F_i - \sum_{i=2}^{i=N-1} F_i\right]\\ &\qquad n = 3, 4, \ldots, N\end{aligned}\right\} \quad (38)$$

where

$$F_n = \left(\frac{N_\xi}{Eh} - \nu\frac{N_\theta}{Eh} + \frac{N_T}{Eh}\right)(\sin\varphi_0 - \tilde{\beta}\cos\varphi_0) - \beta\cos\varphi_0 - \frac{\tilde{\beta}^2}{2}\sin\varphi_0 \quad (39)$$

General Computer Program

The equations presented in this paper have been programed in Fortran language on an IBM 7090 high-speed digital computer (General Dynamics/Astronautics production program No. 2682-Sphere). A simplified flow diagram of the computer program is shown in Fig. 4, and a brief description of the program follows.

As shown in the flow diagram, the necessary nondimensional input to the program consists of geometry, temperature parameters, physical loads, boundary conditions, and a suitable convergence tolerance. The mesh size selection is generally made in accordance with the remarks made by Sepetoski.[7] Output consists of the basic dependent variables Ψ and β along with appropriate nondimensional components of displacement and stress. After the first iteration, which gives the linear (i.e., small deflection) solution, the nonlinear terms in the physical loads and boundary conditions are introduced by an appropriate iteration loop. A convergence test is made after each iteration. It was decided to base convergence on an admissible percent error between successive iterations of any or all of the three nonlinear values of Ψ, β, and u/h evaluated at any two points. The iterations are continued until all of the convergence criteria are satisfied; then the program computes the nonlinear output. Iterations 1, 2, m, and $m + 1$, where m represents the number of iterations to convergence, are printed out in detail. In addition, a table giving values of the convergence functions for every intermediate iteration is printed out. If required, the program can compute and print out a specified number of iterations rather than iterate until convergence.

It can be seen from the steps outlined previously that a considerable number of functions are required, each of which has as many values as there are mesh points. However, only about 20,000 core storage locations of the 7090 can be allocated for storage of these functions. Consequently, since the program is required to accommodate as many as 20,000 mesh points, the use of mediary tapes was essential. By means of storage tapes, each function was split into groups (logical records). Only one group is in core at any time. Ideally 11 tapes should be used; however, only 10 are available. Thus one tape is re-used, the initial information on it being written over. The program was written as a "chain-job" with 4 main programs using 12 subroutines. Execution time varies widely and depends primarily upon the number of mesh points and iterations to convergence.

III. Solution of a Nonclassical Problem

Computer Input Data

In this section, a nonclassical problem involving a spherical shell of variable thickness with a hole at the apex is solved by means of the computer program. The problem itself is somewhat artificial; however, because of its generality it serves as an excellent example for the purposes of explaining important aspects of the analysis technique.

Consider a spherical shell with the geometry shown in Fig. 5, and let

$$(\varphi_0)_1 = 10^\circ \qquad (\varphi_0)_N = 60^\circ \qquad \bar{\Delta s} = 1.25$$
$$\rho_1 = 1500 \qquad \nu = 0.3 \tag{40}$$
$$h = h_1[1 + \sin(\varphi_0 - 10^\circ)]$$

Consequently, it easily may be shown that

$$\left.\begin{aligned} N = 1048 \qquad \rho &= 1500/1 + \sin(\varphi_0 - 10^\circ) \\ \bar{h} &= 1 + \sin(\varphi_0 - 10^\circ) \\ h' &= \tfrac{1}{1500}\cos(\varphi_0 - 10^\circ) \\ hh'' &= -[1/(1500)^2][1 + \sin(\varphi_0 - 10^\circ)] \times \\ &\qquad \sin(\varphi_0 - 10^\circ) \end{aligned}\right\} \tag{41}$$

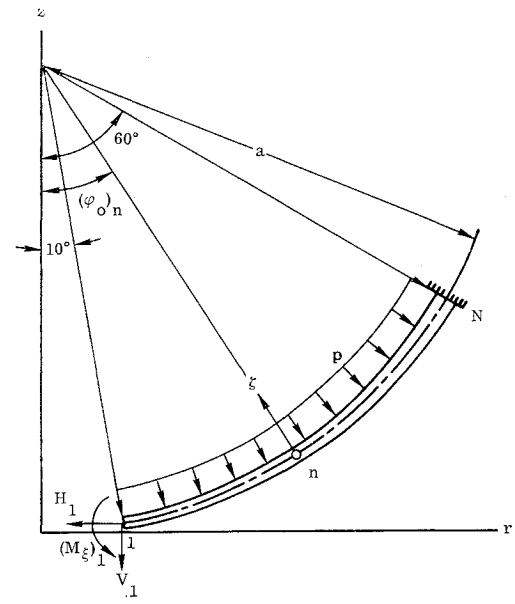

Fig. 5 Geometry and loading for general problem.

Let the temperature be given by the relation

$$kT = A + B\zeta \tag{42}$$

where

$$A = -0.0003\,[1 - \sin(\varphi_0 - 10^\circ)] \tag{43}$$
$$B = -2A/h$$

Thus, with Eqs. (2), it follows that

$$\left.\begin{aligned} N_T/Eh &= -0.00\,03\,[1 - \sin(\varphi_0 - 10^\circ)] \\ N_T'/E &= (0.0003/\rho)\cos(\varphi_0 - 10^\circ) + h'(N_T/Eh) \\ M_T/Eh^2 &= 0.00005\,[1 - \sin(\varphi_0 - 10^\circ)] \\ M_T'/Eh &= -(0.00005/\rho)\cos(\varphi_0 - 10^\circ) + \\ &\qquad 2h'(M_T/Eh^2) \end{aligned}\right\} \tag{44}$$

Assume that the shell is loaded by a constant pressure p that acts normal to the middle surface as shown in Fig. 5. Consequently

$$p_V = -p\cos\varphi \qquad p_H = p\sin\varphi \tag{45}$$

hence

$$p_V/E = -(p/E)[\cos\varphi_0 + \beta\sin\varphi_0 + 0(\beta^2)]$$
$$p_H/E = (p/E)[\sin\varphi_0 - \beta\cos\varphi_0 + 0(\beta^2)] \tag{46}$$

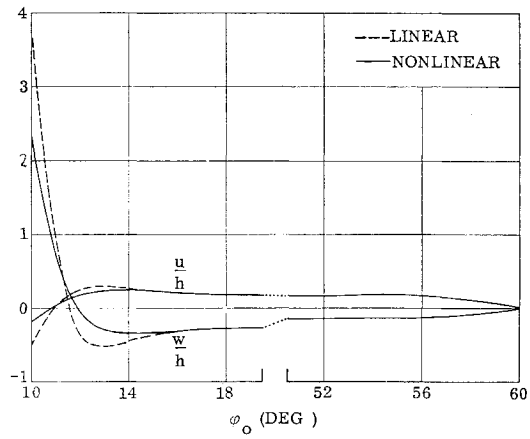

Fig. 6 Nondimensional displacement components.

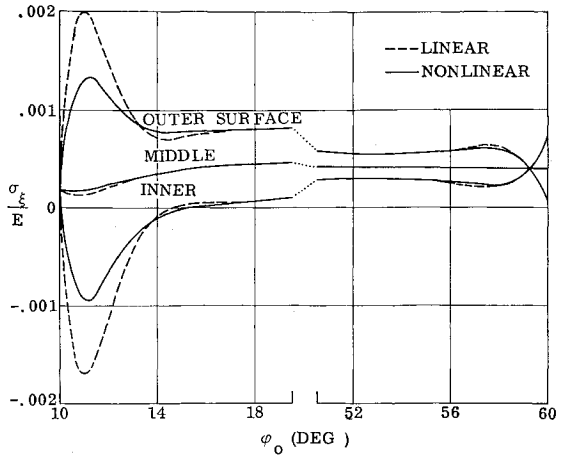

Fig. 7 Nondimensional meridional stresses.

A value of

$$p/E = 1 \times 10^{-6} \tag{47}$$

was selected for this numerical example, and a nondimensional line load of intensity

$$(V/Eh)_1 = 1 \times 10^{-6} \tag{48}$$

was assumed to act as shown in Fig. 5. With these values, it follows from Eqs. (9) that the physical input loads become

$$\left.\begin{aligned} \frac{V}{Eh} &= \frac{10^{-6}}{\bar{h}}\frac{(\sin\varphi_0)_1}{\sin\varphi_0} - \frac{\overline{\Delta s}}{\bar{h}}\frac{1}{\sin\varphi_0}\times \left[\frac{1}{2}(g_1+g_n)+\sum_{i=2}^{i=n-1} g_i\right] \\ g_n &= -10^{-6}(\cos\varphi_0+\tilde{\beta}\sin\varphi_0)\sin\varphi_0 \\ \frac{V'}{E} &= -\left(\frac{V}{Eh}\right)\frac{\cot\varphi_0}{\rho}+10^{-6}(\cos\varphi_0+\tilde{\beta}\sin\varphi_0) \\ (p_H/E) &= 10^{-6}(\sin\varphi_0-\tilde{\beta}\cos\varphi_0) \\ \frac{hp_H'}{E} &= 10^{-6}\left[\frac{\cos\varphi_0}{\rho}+\frac{\tilde{\beta}}{\rho}\sin\varphi_0-\frac{\tilde{h}}{2\overline{\Delta s}}\times (\beta_{n+1}-\beta_{n-1})\cos\varphi_0\right] \end{aligned}\right\} \tag{49}$$

A stress resultant H_1 and stress couple $(M_\xi)_1$ with magnitudes

$$(H/Eh)_1 = 2 \times 10^{-4} \qquad (M_\xi/Eh^2)_1 = 3 \times 10^{-5} \tag{50}$$

are applied as shown in Fig. 5. Also, the shell is clamped at

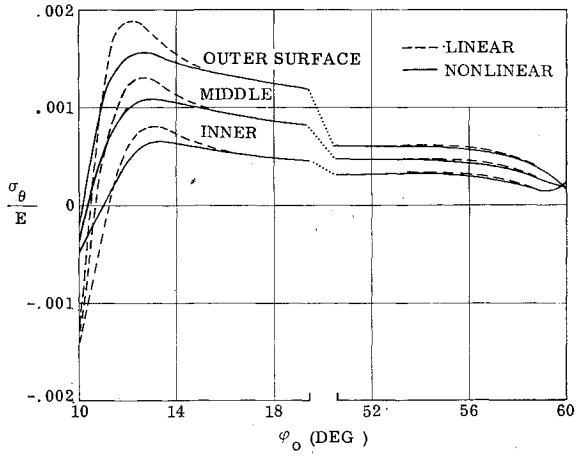

Fig. 8 Nondimensional hoop stresses.

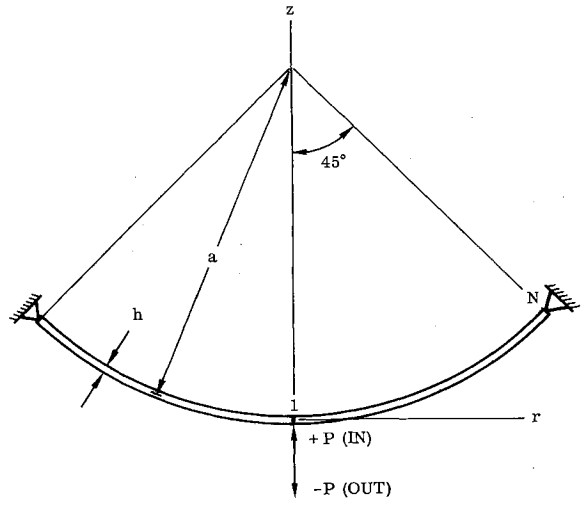

Fig. 9 Concentrated loading at apex of spherical shell.

the terminal point N; consequently the boundary conditions at N are

$$(u/h)_N = \beta_N = 0 \tag{51}$$

In this instance, owing to the constraints at N, it is convenient to impose the condition

$$(w/h)_N = 0 \tag{52}$$

It was decided to base the following convergence tolerance on β_1:

$$|\{1 - [(\beta_1)_{m-1}/(\beta_1)_m]\} \times 100| \leq 0.015\% \tag{53}$$

where m is the number of iterations to convergence.

Numerical Results

With the input data specified by Eqs. (40–53), the quantities shown in the flow diagram were computed. For the present problem, 52 iterations were required to provide con-

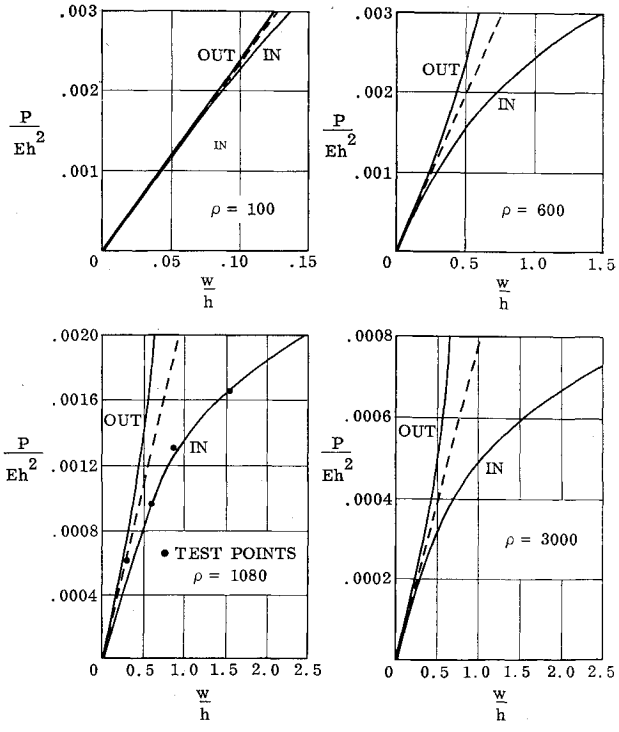

Fig. 10 Load-deflection curves for various radius-thickness ratios.

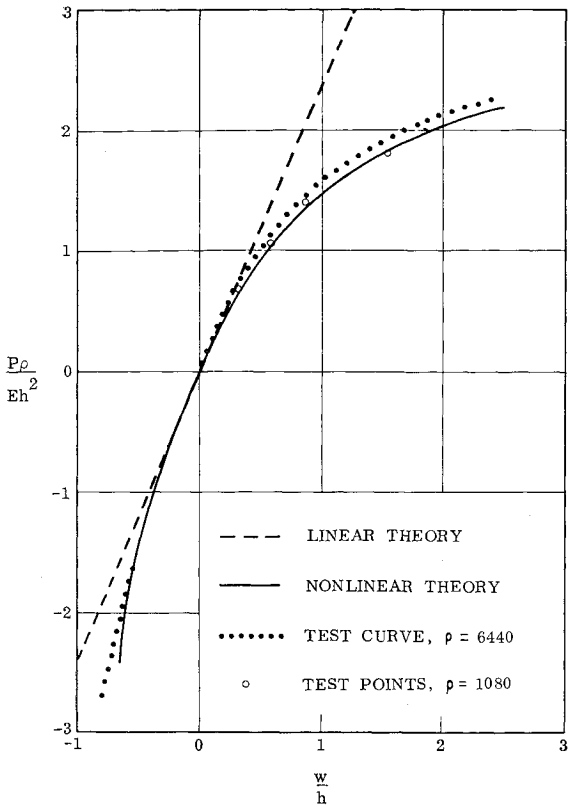

Fig. 11 Composite load-deflection curve.

vergence; accordingly the total 7090 time (compilation, loading, and execution) was very nearly 30 min.

Nondimensional output data consisting of components of displacement and stress may be plotted vs the angle φ_0, as shown in Figs. 6–8. Note that nonlinear effects are important in the narrow edge-zone $10° \leq \varphi_0 < 16°$. However, for $16° < \varphi_0 \leq 60°$, the linear and nonlinear theory gave results that were in close agreement. Also, observe that, in this instance linear theory usually gives conservative results.

IV. Deep Spherical Shell with Point Load at Apex

Computer Input Data

As another numerical example, consider a spherical shell of constant thickness supported as shown in Fig. 9. Assume

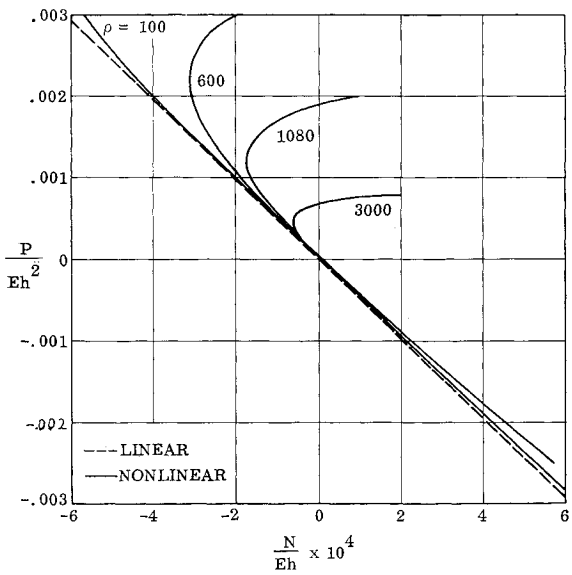

Fig. 12 Load-membrane stress curves for various radius-thickness ratios.

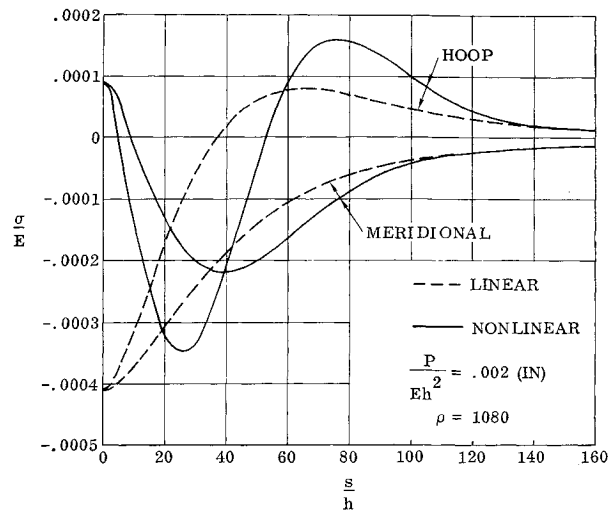

Fig. 13 Nondimensional membrane stresses.

that the shell is loaded at the apex by a vertical concentrated force P that may act "inward" or "outward." Take

$$(\varphi_0)_1 = 0 \qquad (\varphi_0)_N = 45° \qquad \overline{\Delta s} = \bar{h} = 1 \tag{54}$$

$$\nu = 0.3$$

and let it be required to find solutions for the geometric parameters $\rho = 100$, 600, 1080, and 3000. Accordingly the pertinent input loads and boundary conditions assume the form

$$\frac{V}{Eh} = -\frac{1}{2\pi\rho \sin\varphi_0} \cdot \frac{P}{Eh^2} \qquad \frac{V'}{E} = -\frac{V}{Eh} \cdot \frac{\cot\varphi_0}{\rho} \tag{55}$$

$$\Psi_1 = \beta_1 = 0 (a_1 = a_2 = b_1 = b_2 = 0) \tag{56}$$

$$(u/h)_N = (M_\xi/Eh^2)_N = (w/h)_N = 0$$

A convergence tolerance on values of Ψ_2 and β_2 is taken to be

$$|\,\%\text{ error } \Psi_2 \text{ or } \beta_2\,| \leq 0.025\% \tag{57}$$

Numerical and Experimental Results

As before, with the input data specified by Eqs. (54–57), the quantities shown in the flow diagram (Fig. 4) were computed. Selected portions of the output data may be plotted as shown in Figs. 10–15. In each instance, the solid and dashed lines represent results obtained on the basis of nonlinear and linear theory, respectively.

In Fig. 10, the absolute value of the load parameter P/Eh^2 is plotted vs the absolute value of the vertical deflection w at the apex divided by the shell thickness h. For reasonable loads, observe that nonlinear effects become more pro-

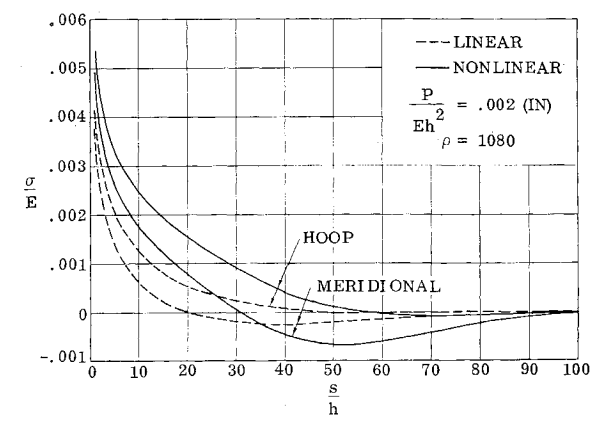

Fig. 14 Nondimensional bending stresses.

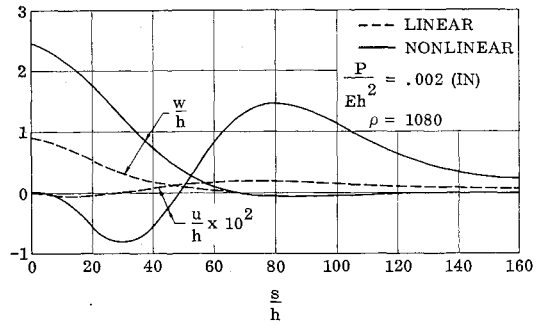

Fig. 15 Nondimensional displacement components.

nounced as ρ increases. Also note, within the framework of large deflection theory, that it is often necessary to distinguish carefully between inward and outward bending, whereas on the basis of small deflection theory no such distinction is required. In particular, linear theory is conservative for outward deflections but unconservative for inward deflections.

The results shown in Fig. 10 may be presented in a more compact and usable form by plotting $P\rho/Eh^2$ vs w/h, as shown in Fig. 11. Note, for all practical purposes, that only two curves result. Therefore, the information given in Fig. 11 is valid for all values of ρ. This rather surprising result is explained easily by noting that significant deformation takes place only in a narrow edge-zone near the loaded apex. Under these circumstances, nonlinear shallow shell theory applies, for which the fundamental load parameter is $P\rho/Eh^2$. To support this assertion, it may be observed that the nonlinear curve shown in Fig. 11 for positive values of P is in excellent agreement with shallow shell results,[16] for which the significant deformation takes place in a narrow boundary layer near the apex. In addition, the linear results given in Figs. 10 and 11, as well as Figs. 12–14, agree with a linear shallow shell analysis given by Reissner.[26]

The following simple formula, which was obtained by a hyperbolic curve fit[31] of the theoretical nonlinear results given in Fig. 11, is valid for both inward and outward loads and should prove to be of considerable usefulness in actual practice:

$$\frac{w}{h} = \frac{P\rho}{Eh^2}\left[0.1 + \frac{1}{3.16 - (P\rho/Eh^2)}\right] \tag{58}$$

$$-2.40 < \frac{P\rho}{Eh^2} < 2.25$$

Two load-deflection tests (Fig. 16) were run on hydrodynamically bulged spherical shells with the geometry and material properties given in Table 1. Specimen A (ρ = 6440) was set up in an Instron testing machine, and load vs both inward and outward deflections

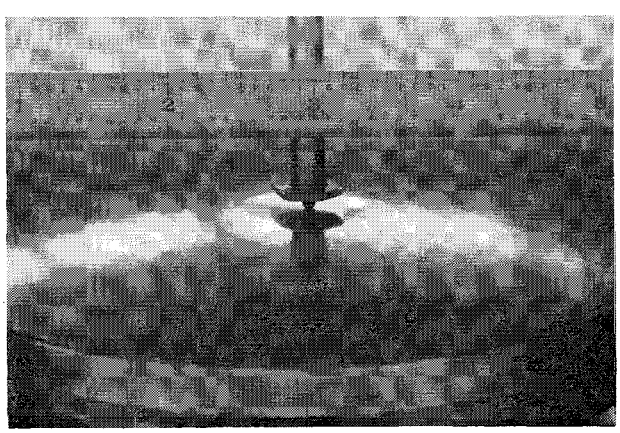

Fig. 16 Spherical shell point load test, ρ = 6440.

Table 1 Geometry and material properties of spherical shells used in tests

	Specimen A (Fig. 16)	Specimen B
Material (steel)	AISI 321	AISI 321
E, psi	28×10^6	25×10^6
Apex angle, deg.	14.4	90
a, in.	10.3	9
h, in.	0.0016	0.0083
ρ	6440	1080
Edge restraint	Glued to ring	None
Pointer radius, in.	$\frac{1}{16}$	$\frac{3}{64}$

(machine head travel) was automatically recorded. A similar procedure was used for specimen B (ρ = 1080), but deflections were measured only at specified values of inward load. Four runs were made for each specimen, and loading and unloading data were averaged and plotted as shown in Fig. 11. Obviously there is excellent correlation between theoretical and experimental results. This lends credence to nonlinear shell theory itself and also substantiates the accuracy of the numerical integration technique used in this paper.

Figure 12 contains a plot, for various values of ρ, of P/Eh^2 vs the dimensionless membrane stress parameter N/Eh evaluated at the apex. For outward deflections, the results obtained from both linear and nonlinear theory display the same trend and differ by only a few percent. However for nonlinear inward deflections, note, for larger values of ρ, that N/Eh initially takes on compressive values but then "decreases" and eventually becomes tensile.

In Figs. 13–15 are shown typical numerical results (P/Eh^2 = 0.002, ρ = 1080), which give the variation of nondimensional components of membrane stress, bending stress, and displacement components with the nondimensional meridional distance s/h measured from the apex. Note that pertinent stress and displacement quantities rapidly deteriorate as s/h increases and observe the bending stress singularity at the apex. These results vividly illustrate the fact that results based on linear theory can be very misleading.

V. Closure

Both the numerical results and experimental evidence given in this paper exemplify the scope and validity of the proposed analysis technique. Accordingly, it now is possible to treat a wide class of problems that involve large axisymmetric deflections of spherical shells. It was shown that large deflection effects can be of considerable practical importance and that linear theory may or may not be conservative, depending upon the geometry and type of loading. It is evident that nonlinear shell theory, where appropriate, should be incorporated eventually into standard design practices for stress problems concerning aerospace vehicle shell structures.

References

[1] Berardi, G., "Risoluzione alle differenze finite del problema della lastra curva a simmetria assiael," Genie Civil **95**, 766–782 (1957).

[2] Galletly, G., "Edge influence coefficients for toroidal shells of positive Gaussian curvature," J. Eng. Ind. **82**, 60–68 (1960).

[3] Galletly, G., "Edge influence coefficients for toroidal shells of negative Gaussian curvature," J. Eng. Ind. **82**, 69–75 (1960).

[4] Galletly, G., Kyner, W., and Moller, C., "Numerical methods and the bending of ellipsoidal shells," J. Soc. Ind. Appl. Math. **9**, 489–513 (1961).

[5] Kraus, H., Bilodeau, G., and Langer, B., "Stresses in thin-walled pressure vessels with ellipsoidal heads," J. Eng. Ind. **83**, 29–42 (1961).

[6] Hubka, R., "A generalized finite-difference solution of axisymmetric elastic stress states in thin shells of revolution," Space Technology Lab. Rept. 7106-0066-NU-000 (1961).

[7] Sepetoski, W., Pearson, C., Adkins, A., and Dingwell, I., "A digital computer program for the general axially symmetric thin-shell problem," J. Appl. Mech. **84**, 655–661 (1962).

[8] Radkowski, P., Davis, R., and Bolduc, M., "Numerical analysis of equations of thin shells of revolution," ARS J. **32**, 36–41 (1962).

[9] Keller, H. and Reiss, E., "Iterative solutions for the nonlinear bending of circular plates," Comm. Pure Appl. Math. **11**, 273–292 (1958).

[10] Keller, H. and Reiss, E., "Spherical cap snapping," J. Aerospace Sci. **26**, 643–652 (1959).

[11] Thurston, G., "A numerical solution of the non-linear equations for axisymmetric bending of shallow spherical shells," J. Appl. Mech. **28**, 557–568 (1961).

[12] Mushtari, Kh., and Galimov, K., *Nonlinear Theory of Thin Elastic Shells* (Tatknigoizdat, Kazan, U.S.S.R., 1957); also NASA TT-F62 (1961).

[13] Wilson, P. and Spier, E., "Numerical analysis of small finite axisymmetric deformation of thin shells of revolution," General Dynamics/Astronautics Engineering Research Rept. ERR-AN-153 (1962).

[14] Wilson, P. and Spier, E., "Numerical analysis of small finite axisymmetric deformation of thin shells of revolution," *Proceedings of the Fourth International Symposium on Space Technology and Science* (Publications Trading Co., Tokyo, 1962), pp. 170–193.

[15] Wilson, P., Spier, E., and Rose, H., "A computer program for the analysis of large axisymmetric deflections of spherical shells," General Dynamics/Astronautics Rept. ERR-AN-234 (1963).

[16] Archer, R., "On the numerical solution of the nonlinear equations for shells of revolution," J. Math. Phys., **41**, 165–178 (1962).

[17] Newman, M. and Reiss, E., "Axisymmetric snap buckling of conical shells," NASA TN-D-1510, pp. 451–462 (1962).

[18] Hwang, C., "Non-linear pressure vessel stress analysis using the optimum programming approach," AIAA J. **1**, 2838–2840 (1963).

[19] Reissner, E., "On the theory of thin elastic shells," *Reissner Anniversary Volume* (J. W. Edwards Brothers, Inc., Ann Arbor, Mich., 1949), pp. 231–247.

[20] Reissner, E., "On axisymmetrical deformations of thin shells of revolution," Proc. Symp. Appl. Math. **3**, 27–52 (1949).

[21] Biezeno, C., "Uber die Bestimmung der Durchschlagkraft einer schwach-gekrummten kreisformigen Platte," Z. Angew Math. Mech. **15**, 10–22 (1935).

[22] Chien, W.-Z. and Hu, H.-C., "On the snapping of a thin spherical cap," *Proceedings of the 9th International Congress of Applied Mechanics 6* (University of Brussels, Brussels, Belgium), pp. 309–363 (1957).

[23] Budiansky, B., "Buckling of clamped shallow spherical shells," *Proceedings of the Symposium on the Theory of Thin Elastic Shells* (North-Holland Publishing Co., Amsterdam, the Netherlands, 1960), pp. 64–94.

[24] Weinitschke, H., "On the stability problem for shallow spherical shells," J. Math. Phys. **38**, 209–231 (1959).

[25] Ashwell, D., "On the large deflexion of a spherical shell with an inward point load," *Proceedings of the Symposium on the Theory of Thin Elastic Shells* (North-Holland Publishing Co., Amsterdam, the Netherlands, 1960), pp. 43–63.

[26] Reissner, E., "Stresses and small displacements of shallow spherical shells," J. Math. Phys. **25**, 279–300 (1946).

[27] Potters, M. "A matrix method for the solution of a second order difference equation in two variables," Mathematisch Centrum, Amsterdam, The Netherlands, Rept. MR 19 (1955).

[28] Wilson, P. and Spier, E., "On the direct numerical integration of a system of linear second-order ordinary differential equations," General Dynamics/Astronautics Engineering Research Rept. ERR-AN-341 (1963).

[29] Budiansky, B. and Radkowski, P., "Numerical analysis of unsymmetrical bending of shells of revolution," AIAA J. **1**, 1833–1842 (1963).

[30] Spera, D., "Analysis of elastic-plastic shells of revolution containing discontinuities," AIAA J. **1**, 2583–2589 (1963).

[31] Breuer, F., "A hyperbolic surface fitting procedure," General Dynamics/Astronautics Rept. AE63-0033 (1963).